Antibody-Mimetic Peptoid Nanosheets for Molecular Recognition

Gloria K. Olivier, Andrew Cho,[†] Babak Sanii,[‡] Michael D. Connolly, Helen Tran,[§] and Ronald N. Zuckermann*

The Molecular Foundry, Lawrence Berkeley National Laboratory, 1 Cyclotron Road, Berkeley, California 94720, United States. [†]Present address: Cornell Medical School, New York, New York 10065, United States. [‡]Present address: Keck Sciences Department, Claremont Colleges, Claremont, California 91711, United States. [§]Present address: Department of Chemistry, Columbia University, New York, New York 10027, United States.

ABSTRACT The ability of antibodies to bind a wide variety of analytes with high specificity and high affinity make them ideal candidates as molecular recognition elements for chemical and biological sensors. However, their widespread use in sensing devices has been hampered by their poor stability and high production cost. Here we report the design and synthesis of a new class of antibody-mimetic materials based on functionalized peptoid nanosheets. A high density of conformationally constrained peptide and peptoid loops are displayed on the surface of free-floating nanosheets to generate an extended, multivalent two-dimensional material that is chemically and biologically stable. The nanosheet serves as a robust, high-surface area scaffold upon which to display a wide variety of functional loop sequences. The functionalized nanosheets were characterized by atomic force microscopy, X-ray diffraction, and X-ray reflectivity measurements, and were shown to serve as substrates for enzymes (protease and casein kinase II), as well as templates for the growth of defined inorganic materials (gold metal).

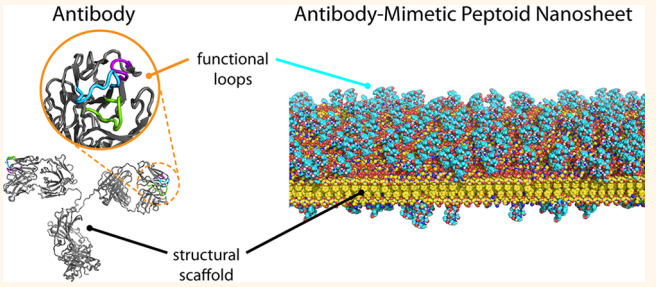

KEYWORDS: protein-mimetic materials · molecular recognition · loop display · two-dimensional nanomaterials · bioinspired polymers

Antibodies are exceptional at molecular recognition, capable of recognizing a breadth of antigens with both high specificity and high affinity.[1] Antibodies have thus become a vital reagent in healthcare and biotechnology applications, as well as components in chemical and biological sensors.[2,3] However, significant technical challenges continue to hamper the efficient manufacturing and deployment of antibodies in devices, including poor solubility, lack of temperature and enzyme stability, and improper folding when expressed in bacteria.[4] These limitations, coupled with the desire to rapidly engineer antibodies against novel targets, have fueled the need for more stable and cost-effective alternatives to natural antibodies and attracted recent interest toward the development of easy-to-manufacture antibody mimics.[4−8]

One of the most promising approaches to engineering antibody mimics has been to transfer the essential molecular recognition features of a natural antibody onto a smaller, well-behaved protein.[4] The natural antibody is comprised of two parts: (1) a rigid scaffold, and (2) a cluster of flexible peptide loops displayed atop the scaffold (Figure 1A). While the scaffold remains largely constant from one antibody to the next, the loop sequences are highly variable, chemically tailored to bind the antigen target with specificity and high affinity. In addition to providing chemical diversity, the cluster of loops work together to form a convergent antigen binding site. Inspired by this architecture, current efforts to engineer antibody mimics typically follow a common design strategy where several polypeptide loops are displayed on the surface of a small, easy-to-manufacture protein scaffold (Figure 1B,C). This simplified architecture aims to capture the specificity and multiloop display of the antibody binding site while improving upon its solubility, bioavailability, bacterial expression, and production costs. Examples of protein-based antibody mimicry include grafting a single antigen-recognition loop onto a smaller, easier-to-fold scaffold,[9] as well as screening combinatorial libraries of well-behaved

* Address correspondence to rnzuckermann@lbl.gov.

Received for review July 26, 2013 and accepted September 9, 2013.

Published online September 09, 2013
10.1021/nn403899y

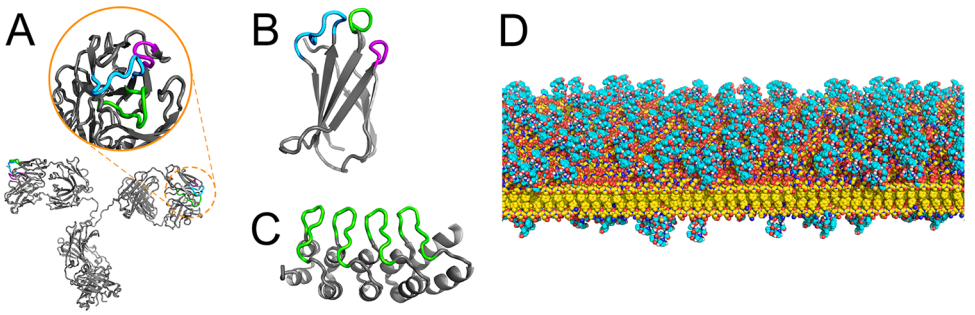

Figure 1. Architecture of an (A) anti-canine lymphoma IgG2 antibody (PDB code: 1IGT), (B) antibody-mimetic loops on a fibronectin scaffold (PDB code: 2OBG), (C) antibody-mimetic loops on an ankyrin repeat protein scaffold (PDB code: 1SVX), and (D) a high density of antibody-mimetic loops displayed on a peptoid nanosheet scaffold.

small proteins that have been engineered to display randomized, surface-exposed loops.[10] While protein-based antibody mimics show great promise, they are susceptible to denaturation at extreme pH and temperatures and are easily degraded by proteases likely to be encountered in samples of biological origin.

We present a new class of antibody-mimetic material, built from a rugged peptoid nanosheet scaffold (Figure 1D). Peptoids are bioinspired, sequence-specific polymers capable of folding into protein-like architectures.[11−15] However, unlike proteins, peptoids are made from protease-resistant building blocks, cheap to manufacture, and offer access to a vast diversity of chemical functionalities.[15] Recently, peptoid sequences have been designed to self-assemble into highly stable, two-dimensional (2D) nanosheets in water.[16] The nanosheets are hundreds of micrometers in length and width, yet only two molecules (3 nm) thick, as characterized with aberration-corrected electron microscopy, atomic force microscopy (AFM), and X-ray diffraction (XRD).[14,16,17] Peptoid nanosheets provide a unique opportunity to merge the molecular recognition properties of proteins with the rugged utility of synthetic, 2D nanomaterials.[18,19] The nanosheets are a readily functionalizable, high surface area 2D platform on which to display a high density of molecular recognition sites on both faces of the sheet. Moreover, peptoid nanosheets are stable in air or water, do not aggregate in solution, and have a hydrophilic zwitterionic exterior surface, a property which is desirable for resisting nonspecific protein adsorption.[20,21]

Here we demonstrate that peptoid polymers of specific sequence can be programmed to self-assemble, or "fold", into an antibody-like architecture: a peptoid nanosheet scaffold decorated with surface-exposed loop domains. The formation of loops on the surface of the nanosheet was confirmed by AFM and X-ray scattering, as well as by chemical and biological function. We show that biologically active peptides can be inserted into the linear peptoid sequence, and that peptide loops displayed on a peptoid nanosheet scaffold are accessible for molecular recognition by proteases and casein kinase II. In addition to biorecognition, we also highlight the utility of loop-displaying peptoid nanosheets as 2D templates to nucleate the "bottom-up" growth of gold nanostructures.

RESULTS AND DISCUSSION

Design and Synthesis of Antibody-Mimetic Peptoid Nanosheets. An efficient strategy for programming loop display into a peptoid nanosheet is derived from knowledge of the previously reported[17] mechanism of nanosheet formation. Peptoid nanosheets are produced by a hierarchical mechanism, first involving adsorption of amphiphilic peptoids into a monolayer at the air−water interface, followed by lateral compression of the monolayer into an ordered, irreversible peptoid bilayer (nanosheet).[17] The air−water interface plays a critical role in preorganizing the polymer chains prior to compression into the bilayer, a role which can be exploited to add functionality to the nanosheet scaffold. The interface drives the amphiphilic peptoid to orient specific functional groups on the aqueous and air sides of the peptoid monolayer, which ultimately become the exterior and interior faces of the peptoid nanosheet, respectively. Therefore, we reasoned that short loops could be selectively displayed on the water-exposed face of the nanosheet by inserting a linear segment of hydrophilic residues into the middle of the linear sheet-forming strand (Figure 2). Placing the loop sequence in the middle of the strand, between two amphiphilic sheet-forming segments, should anchor the ends of the loop to the air−water interface. During compression of the peptoid monolayer, the amphiphilic segments of the polymer are designed to align and pack tightly with neighboring strands, drawing the hydrophilic insert into the shape of a loop (Figure 2). Additionally, the use of a single-chain sequence design avoids the technical challenges associated with covalently coupling loop domains onto the surface of preformed peptoid nanosheets, including incomplete loop coupling (loose ends), lack of conformational control (tangled and interlocking loops), and purification or removal of unreacted coupling reagents.

To study the impact of inserting a hydrophilic loop domain on peptoid nanosheet formation, we synthesized a length series, where the number of residues in the loop insert (n) was systematically varied (n = 0, 4, 8, and 12) while keeping the length and composition of the sheet-forming motif constant (compounds **1**–**4**, Table 1). The loop insert was initially a homopolymer of *N*-(2-methoxyethyl)glycine (Nme) residues for the purposes of hydrophilicity and ease of synthesis. Nanosheets were prepared from each peptoid using the vial-rocking method described previously[17] and characterized by optical microscopy, AFM, and powder XRD. All sequences of the length series (**1**–**4**) were capable of assembling into peptoid nanosheets. By optical microscopy, nanosheets prepared from the loop-forming peptoids exhibited sharp, straight edges and appeared qualitatively similar in size and shape (see Figures 5 and 6) to previously reported peptoid nanosheets lacking a loop-forming domain.[14,16,17] Even the longest of the three loops tested (peptoid **4**), for which the loop accounts for 30% of the overall chain length, is capable of assembling into nanosheets. The optical microscopy results confirm that introducing a hydrophilic segment into the amphiphilic sequence of **1** does not prevent peptoid nanosheet formation. Thus, inserting a hydrophilic functional domain into the middle of the chain is a viable strategy for encoding additional information content into a single-chain, nanosheet-assembling peptoid.

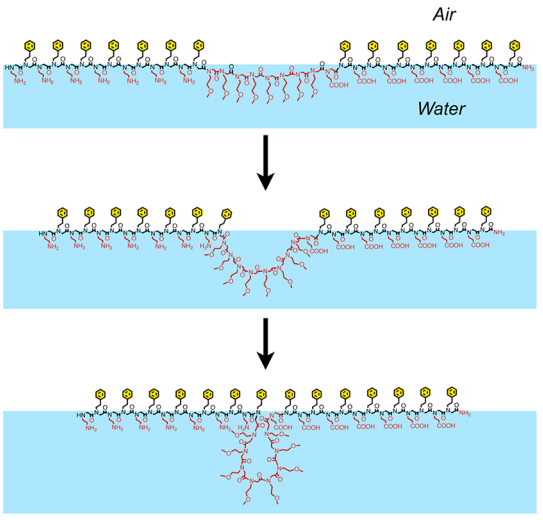

Figure 2. Mechanism of folding a linear peptoid sequence into a loop domain through compression of the peptoid monolayer at the air–water interface.

Evidence of Loop Display. To confirm the presence of loops on the surface of the nanosheets, AFM was used to probe the thickness and surface morphology of individual nanosheets. The nanosheets prepared from loop-forming peptoids are thicker and have greater

TABLE 1. Peptoid Sequences for Studying Loop Formation (1–4) and Peptoid–*Peptide* Hybrid Sequences for Studying Loop Function (5–8)[e]

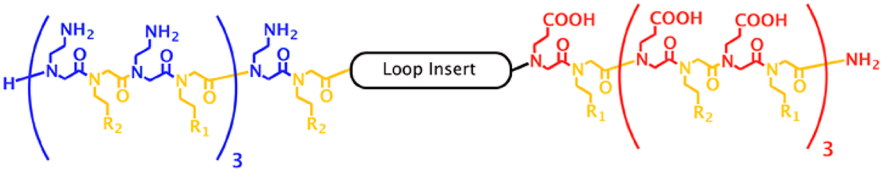

Peptoid	Overall Chain Length (Loop Size)[a]	R_1[b]	R_2[c]	Loop Insert[d]	Expected Molecular Weight (Observed)[f]
1	28 (0)	Ph	Ph	No loop insert	3878.5 (3878.6)
2	32 (4)	Ph	Ph	—(Nme)$_4$—	4339.0 (4339.8)
3	36 (8)	Ph	Ph	—(Nme)$_8$—	4799.5 (4799.8)
4	40 (12)	Ph	Ph	—(Nme)$_{12}$—	5260.6 (5257.5)
5	40 (12)	Ph	Ph	—Nme–βAla–Glu–Glu–Glu–Ser–Gly–Gly–Glu–βAla(Nme)$_2$—	5083.7 (5083.5)
6	38 (10)	Ph	Ph	—Nme–βAla–Lys–Thr–Gln–Ala–Ser–βAla(Nme)$_2$—	4881.6 (4881.0)
7	38 (10)	Ph	Biph	—Nme–βAla–Lys–Thr–Gln–Ala–Ser–βAla(Nme)$_2$—	5444.3 (5444.0)
8	28 (0)	Ph	Biph	No loop insert	4411.1 (4411.5)

[a] Loop Size is defined as the number of residues in the Loop Insert. [b] Ph = phenyl. [c] Biph = biphenyl. [d] Nme = *N*-(2-methoxyethyl)glycine; βAla = beta alanine. [e] Polar residues in the amphiphilic sheet-forming domains of the polymer are colored blue and red; aromatic residues in the amphiphilic domains are colored yellow. [f] as determined by MALDI mass spectrometry.

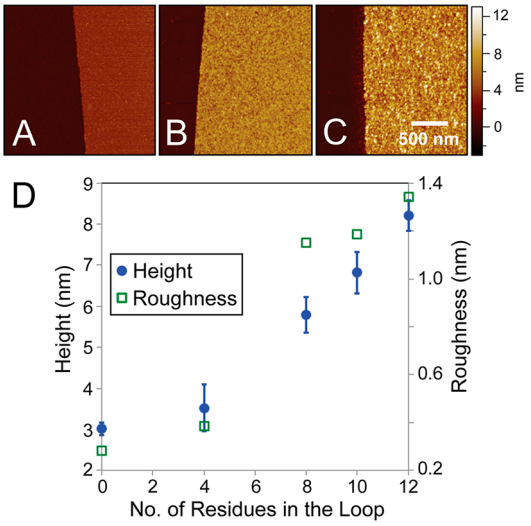

Figure 3. Atomic force microscopy (AFM) image of the edge of an individual peptoid nanosheet made from (A) peptoid 1 with no loop domain, (B) peptoid 3 with 8 residue loop, and (C) peptoid 4 with 12 residue loop. Nanosheets are deposited on mica and imaged in ambient air. Color scale and lateral scale bar shown with (C) are same for (A) and (B). (D) AFM height and roughness of peptoid nanosheets as a function of loop size.

surface roughness than nanosheets prepared from **1**, lacking the loop-forming motif (Figure 3). Interestingly, the thickness of the loop-containing nanosheets increases with increasing loop size (Figure 3D). The observed relationship between loop size and nanosheet thickness suggests that the majority (if not all) of the residues in the loop get pushed outward, onto the surface of the nanosheet, during nanosheet assembly. In this way, the inserted residues directly contribute to increasing the overall thickness of the nanosheet. Additionally, the roughness of the loop-containing nanosheets, observed by AFM, suggests that the exterior structure of loop-containing nanosheets is more disordered than that of unfunctionalized nanosheets.

To examine the molecular structure of the loop-displaying nanosheets, powder XRD analysis was performed. The XRD spectra, obtained from dry, pelleted stacks of nanosheets, reveal that three-dimensional, loop-displaying nanosheets possess the same degree of molecular order as previously reported 2D peptoid nanosheets.[14,16,17] The diffraction pattern of nanosheets prepared from **3** exhibits a characteristic 4.6 Å peak, attributed to interbackbone spacing between polymer chains, as well as a 2.8 nm peak, arising from the thickness of the peptoid bilayer, underlying the loop domains (Figure S1, Supporting Information). These peaks appear in the XRD analysis of unfunctionalized nanosheets prepared from **1**, and all previously studied nanosheet-forming peptoid sequences also lacking a loop-forming domain.[14,16,17] Thus, the XRD data obtained from **3** indicates that the interior scaffolding of loop-displaying nanosheets consists of an ordered, 2.8 nm thick peptoid bilayer, structurally identical to the bilayer of nonloop-displaying peptoid nanosheets.[16,17] However, nanosheets prepared from **3** exhibited a 5.8 nm thickness, significantly thicker than nonloop-displaying nanosheets, when measured by AFM. The discrepancy in nanosheet thickness detected by these two techniques provides further evidence that the surface-displayed loops are amorphous (disordered), and therefore do not give rise to a discrete diffraction peak in the XRD pattern. Instead, the loop-displaying nanosheets prepared from **3** exhibit noticeably higher scattering intensity in the q = 0.25−1.5 Å^{-1} range than **1**, which is indicative of diffuse scattering from the randomly oriented, disordered loop domains of **3**. Lastly, XRD analysis confirms that insertion of the loop-forming domain does not alter the 4.6 Å lateral, interbackbone spacing between polymer chains, relative to peptoid nanosheets without loops.

While AFM and powder XRD of the peptoid bilayers (nanosheets) are consistent with loop display, loop formation is expected to occur at the air−water interface during compression of the peptoid monolayer (Figure 2). Thus, studying the peptoid monolayer at the air−water interface, prior to collapsing the monolayer into a bilayer,[17] provides a more direct view of loop formation. The surface pressure isotherms of **1** (no loop) and **3** (with 8-residue loop) at the air−water interface confirm that **3** forms a monolayer at the air−water interface, and that the monolayer of **3** follows a similar nanosheet production cycle[17] as **1** (and other previously studied nanosheet-forming peptoid sequences, lacking a loop-forming domain[14,16,17]) during compression and expansion of the air−water interface. The surface pressure data (Figure 4A) provide important confirmation that inserting a hydrophilic loop sequence is compatible with the peptoid nanosheet assembly pathway, and is a general strategy for encoding additional information content into a single-chain, nanosheet-assembling peptoid.

If loops form during compression of the peptoid monolayer, then the monolayer of **3** should be thicker than that of **1**. We probed the thickness of peptoid monolayers prepared from **1** and from **3** at different surface pressures along the compression pathway (Figure 4A) using a Langmuir trough equipped with X-ray reflectivity (XR) capabilities. The electron density in the z-direction (perpendicular to the air−water interface) obtained from these experiments is plotted in Figure 4B. Upon compressing each monolayer to a fixed surface pressure of 37 mN/m, the electron density profiles of **1** and **3** are identical up to 20 Å monolayer depth. However, at depths greater than 20 Å, a distinct, third region of electron density appears in the profile of **3**. The XR data show that **3** assembles into nearly identical alignment in the z-direction as **1**, but possesses an additional layer of polymer, protruding ~1 nm beyond

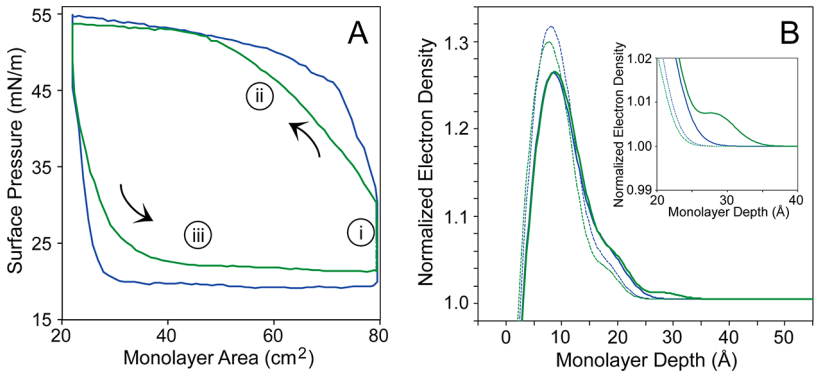

Figure 4. (A) Surface pressure isotherms recorded at room temperature inside a Langmuir trough filled with either 20 μM peptoid 1 (blue) or 20 μM peptoid 3 (green), dissolved in pH 8.0, 10 mM Tris. (i) At the start of each isotherm, the Langmuir trough was held open (monolayer area held constant at 79 cm^2) for 900 s, to allow the peptoid to adsorb into a monolayer at the air−water interface. (ii) Following the adsorption period, the peptoid monolayer was compressed from 79 to 22 cm^2 (by closing the barriers at a rate of 100 cm^2/min), and (iii) then immediately re-expanded (by returning the barriers to the open position). (B) Electron density profiles for monolayers of peptoid 1 (blue) and peptoid 3 (green) obtained from X-ray reflectivity measurements at the air−water interface of a Langmuir trough. Data is normalized by the reflectivity of pure water in air. Dashed and solid curves correspond to the monolayer before and after compression by the Langmuir trough, respectively. Dashed curves were collected after allowing a 20 μM solution of each peptoid (in pH 8.0, 10 mM Tris) to equilibrate at room temperature inside the Langmuir trough for 1.5 h, reaching a surface pressure of 33 mN/m for peptoid 1, and 30 mN/m for peptoid 3. Solid curves were collected after compressing each peptoid monolayer to a fixed surface pressure of 37 mN/m. Inset highlights the region where loop formation is expected to occur.

the monolayer thickness of **1** into the aqueous subphase (Figure 4B). This additional layer of polymer is only observed after the loop-forming peptoid monolayer has been compressed. The position, width, and magnitude of this third region of electron density is consistent with the formation of polymer loops on the aqueous side of the monolayer. In particular, since there is only one pendant loop per polymer strand, the loops are expected to be laterally spaced apart, forming a diffuse layer of polymer, just below the monolayer, that is comprised mostly of water molecules. For this reason, the electron density arising from the loops is only slightly larger than the electron density of water itself and appears as a small, but significant peak in the electron density profile after normalizing the data by the XR of pure water (Figure 4B). Furthermore, the width of this peak arising from compression-driven loop display gives the compressed peptoid monolayer of **3** an overall thickness of 30 Å, in good agreement with one half of the bilayer thickness (58 $\pm$ 4 Å for the bilayer) as determined by AFM of nanosheets prepared with **3** (Figure 3). Therefore, XR measurements provide direct evidence of compression-induced peptoid loop formation at the air−water interface. Compressed monolayers of **1** and **3** also show nearly identical alignment in the *z*-direction, which confirms that insertion of a hydrophilic loop-forming domain does not alter the assembly of the amphiphilic, sheet-forming blocks of the polymer. The surface pressure and XR findings validate our method of loop formation (Figure 2) as a potentially general approach to making a new class of 2D, loop-displaying nanomaterials. Provided that the inserted sequence is sufficiently hydrophilic, our strategy of encoding a linear peptoid for loop formation provides an easy route to display a wide variety of functional peptide or peptoid inserts, in a constrained loop conformation and with a high surface density, on a rugged, 2D peptoid nanosheet platform (Figure 1D).

Molecular Recognition on Antibody-Mimetic Peptoid Nanosheets. The method of loop formation employed here is general enough to display a wide variety of hydrophilic loop sequences on the peptoid nanosheet scaffold. Taking advantage of the growing number of functional peptides that have been discovered by combinatorial display techniques,[22−26] for protein recognition[27] (**5**) and inorganic material recognition[28] (**6** and **7**), we chose several known hydrophilic peptides for insertion into the loop-forming domain. The resulting sequences are peptoid−peptide hybrid polymers, encoded for peptoid nanosheet assembly with peptide loop display. While the 12-residue loops of **4** and **5** both formed nanosheets, the shorter loop of **6** did not. We hypothesized that peptide **6** was not properly anchored by the two amphiphilic sheet-forming segments of the strand during assembly at the air−water interface. Rather than increasing the length of the amphiphilic segments, which is synthetically challenging, we increased the hydrophobicity of the sheet-forming segments, through an alternating sequence of *N*-(2-(4-biphenyl)ethyl)glycine and *N*-(2-phenylethyl)glycine residues on either side of the loop insert (peptoid **7**). The analog of **7** with no loop insert, peptoid **8**, was synthesized as a control. Despite being more hydrophobic than **1**, peptoid **8** readily assembles into nanosheets (Figure 5C). Nanosheets prepared from **8** are 4.5 Å thicker than those prepared from **1**, as determined by AFM (not shown) and powder XRD

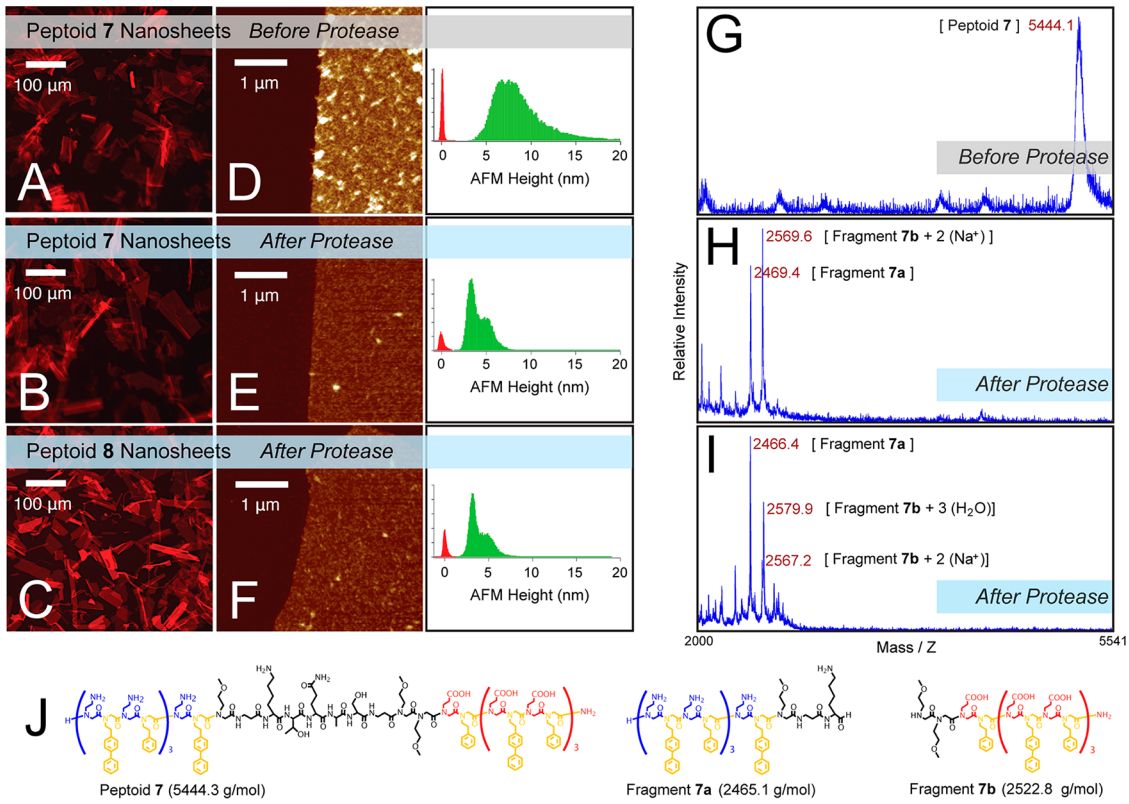

Figure 5. Optical microscopy images of the peptoid 7 nanosheets before (A) and after (B) incubation with protease, in comparison with (C) control peptoid 8 nanosheets without loops. Nanosheets were stained with Nile red prior to optical imaging. AFM image and height distribution (at right of each AFM image), for a representative gold-binding peptide-loop nanosheet before (D) and after (E) incubation with protease, in comparison with (F) the AFM image of a control peptoid 8 nanosheet after incubation with protease. The height distribution is a histogram of the pixel intensities of the AFM image, with mica substrate pixels plotted in red and peptoid nanosheet pixels plotted in green. Matrix-assisted laser desorption/ionization (MALDI) mass spectra of peptoid 7 nanosheets before (G) and after (H) incubation with protease, in comparison with mass spectrum of (I) free-floating, unstructured peptoid 7 after incubation with protease. The nanosheets were dissociated (using acetonitrile) prior to MALDI analysis. (J) Corresponding chemical structures of observed masses.

measurements (Figure S1, Supporting Information). With the exception of the additional 4.5 Å thickness due to the longer 4-biphenylethyl side chain, the aromatic packing of **8** is expected to be similar to that of **1**, as is observable in the crystal structure of a related model compound **9**, *N*,*N*′-bis-(2-phenylethyl)diketopiperazine, prepared from a cyclic dipeptoid (Figure S4, Supporting Information). Thus, the 4-biphenylethyl side chain is a convenient method of modulating the hydrophobicity of the strand and engineering the aromatic interior of the peptoid nanosheet.

To verify peptides can be displayed on a nanosheet surface, as well as highlight the exceptional stability of the nanosheet scaffold, nanosheets prepared from **7** were incubated with a concentrated solution of proteases. If the peptide is displayed properly on the exterior of the nanosheet for molecular recognition applications, then the peptide should be susceptible to proteolysis, resulting in loop degradation and bisection of **7** into two lower molecular weight fragments. Peptoid polymers are known to be stable against proteolytic degradation,[29,30] but it is not known whether nanosheets remain stable or dissociate into soluble polymer strands upon bisection of the peptoid into low molecular weight fragments. The nanosheets made from **7** were incubated with Pronase, a commercially available cocktail of 10 different proteases, and characterized with optical and atomic force microscopy, before and after digestion. Removal of the peptide, and cleavage of the linear peptide-peptoid hybrid polymer into two peptoid fragments, was measured with mass spectrometry (MS). The same pair of cleavage products were detected after digestion of the peptide loop-displaying nanosheets (Figure 5H) as was detected after digestion of free-floating, unstructured polymer strands (Figure 5I). The observed mass fragments correspond to elimination of all but one amino acid residue, and no degradation of the peptoid segments. The MS results demonstrate that peptide loops displayed on the nanosheet surface are accessible for recognition and cleavage by proteases. Similarly, AFM imaging of nanosheets before and after digestion (Figure 5D and E, respectively) reveals that the thickness (and roughness) of nanosheets made from **7** decreases from 7.1 nm (with 2.4 nm roughness) before digestion, to 3.4 nm thick (with 0.5 nm roughness) after

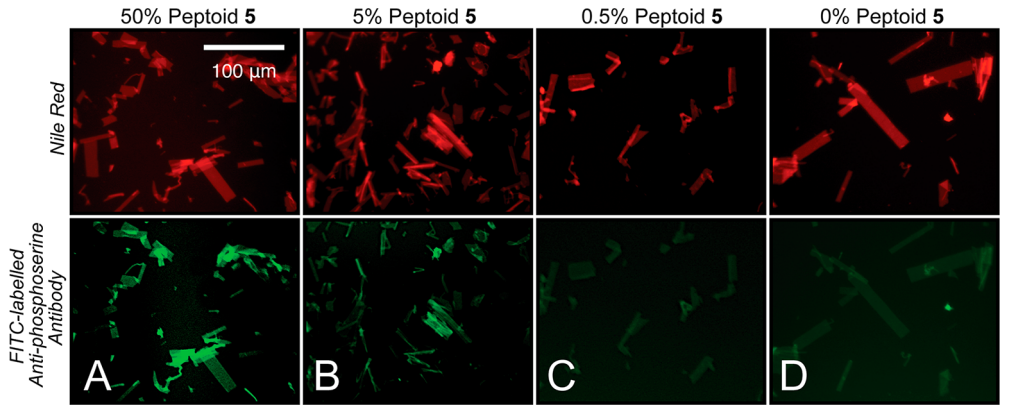

Figure 6. Immunofluorescence imaging of peptide-loop nanosheets after phosphorylation by casein kinase II alpha subunit (CK2α), followed by incubation with FITC-labeled anti-phosphoserine antibody and Nile red dye. Nanosheets are stained uniformly with Nile red, to enable imaging of nanosheets with low or no phosphorylation. Each image was collected using the filters for both dyes: Nile red (top row), and FITC (bottom row). The concentration of peptide loops displayed on the surface of the nanosheet was systematically varied by preparing nanosheets from different mixing ratios of peptoid 1 and peptoid 5 as follows: (A) 50, (B) 5, (C) 0.5, and (D) 0% peptoid 5. Scale bar in (A) is same for all images.

digestion. In fact, the height distribution of proteolyzed **7** nanosheets (histogram, Figure 5E) matches that of control **8** nanosheets (without loops) indicating that: (1) the surface-displayed domains of peptide-loop nanosheets are shaved off by protease, as expected, and (2) the second, smaller peak appearing at 5 nm in the height distribution of both samples (histograms, Figure 5E and F) may be due to a small amount of nonspecific protein adsorption. Optical images of the nanosheets reveal that the size, shape, and abundance of nanosheets is unchanged before (Figure 5A) and after (Figure 5B) cleavage of these peptide loops with protease. By optical microscopy, the proteolyzed peptide–peptoid nanosheets (Figure 5B) are indistinguishable from control nanosheets without loops (Figure 5C). Thus, the structural integrity of the nanosheet scaffold remains intact upon cleavage of the surface-displayed peptide loops. This is remarkable in view of the fact that similarly sized peptoids do not form nanosheets,[16] indicating that the low molecular weight peptoids of digested nanosheets are kinetically trapped in the nanosheet morphology. Taken together, the AFM and MS data obtained with Pronase prove that the peptide loops are accessible for protein binding. In contrast to protein-based antibody mimics, which are susceptible to degradation by proteases, peptoid nanosheets are an exceptionally stable, rugged display material, and offer a simple route to display a high density of linear peptide sequences in constrained, antibody-like loop conformations.

To demonstrate the protein-binding ability of loop-displaying peptoid nanosheets, peptoid nanosheets displaying the consensus peptide for casein kinase II (**5**) were synthesized and incubated with the target protein, casein kinase II (CK2α). Recognition of the peptide substrate by the kinase causes a chemical modification (phosphorylation of the serine residue) of **5**, which can be readily detected with immunofluorescence imaging[25] or gel electrophoresis.[31,32] The consensus peptide substrate for CK2α, in particular, was chosen because it is a heptamer,[27] comprised almost entirely of hydrophilic amino acids. The density of peptide loop display was systematically varied by mixing different ratios of **1** and **5** in solution. Importantly, the mole fraction of each polymer dissolved in the sheet-forming solution is approximately equal to the mole fraction of each polymer incorporated in the nanosheets, as determined by gel electrophoresis (Figure S5, Supporting Information). Nanosheets with varying surface densities of kinase-binding peptide loops, as well as control nanosheets without loops (0% peptoid **5**), were exposed to CK2α and then incubated with a fluorescent, FITC-labeled monoclonal antibody that binds specifically to phosphoserine residues.[33] In contrast to the 0% peptoid **5** nanosheets without loops, which did not bind an appreciable level of the anti-phosphoserine antibody, phosphoserine was visibly detected on the 50 and 5% peptide-loop nanosheets (Figure 6). The brightness of the phosphorylated nanosheets qualitatively decreases with decreasing density of peptide loop display, indicating that the FITC-labeled antibody binds specifically to the peptide loop, rather than nonspecifically to the surface of nanosheets in general. To quantify the degree of phosphorylation occurring at the antibody-mimetic nanosheet surface, relative to free-floating, unstructured peptoid strands, the 50% peptide-loop nanosheets were incubated with CK2α, and then dissociated into individual polymer strands with 0.2% sodium dodecyl sulfate, to enable detection and quantification of the phosphopeptide-peptoid strand by isoelectric focusing gel electrophoresis (Figure 7). The free-floating, unstructured polymer shows 30% conversion to phosphorylated product, when incubated with CK2α. The peptide-loop nanosheets exhibited 20% conversion to phosphorylated product by

CK2α, verifying that peptide loops are accessible for binding and are specifically recognized by CK2α. The difference in reactivity between peptide loops displayed on a nanosheet surface and free-floating, unstructured strands may be due to the fact that the nanosheet is significantly more massive, and therefore diffuse more slowly than an individual polymer molecule in solution.

Beyond protein recognition, loop-displaying peptoid nanosheets also hold promise as a platform for templating the assembly of inorganic components. Mesoscale inorganic–organic composite materials, with hierarchichal order at the nanoscale,[34] offer unique properties that are actively being pursued for a broad range of applications, including light emission, information storage, nanopatterning electronics, and as artificial metalloenzymes.[35,36] The extreme aspect ratio, chemical stability, and atomically defined structure of peptoid nanosheets make them an attractive canvas on which to template metal ions and nanoparticles for use in plasmonic and nanoelectronic applications. With this aim in mind, nanosheets decorated with the gold-binding peptide[28] loop **7** were incubated with an aqueous solution of $[AuCl_4]^-$ ions and monitored with AFM, in order to utilize the surface-displayed loops as nucleation sites for gold nanocrystal growth. In the absence of a reducing agent, the peptide alone has been shown to trigger the formation of gold nanocrystals from $[AuCl_4]^-$ ions, with the crystal morphology highly dependent upon pH and gold ion concentration.[23,37,38] Initial experiments performed with the gold-binding peptide loop nanosheets and $[AuCl_4]^-$ ions at room temperature in pure water yielded nanosheets covered with a continuous, ~50 nm thick metal film (as determined by AFM). In an effort to slow the growth rate of the crystals, and thereby favor the formation of discrete, nanometer-sized gold particles, rather than a continuous film of gold, nanosheets functionalized with the gold-binding peptide loops were incubated with a dilute solution of gold ions at low temperature (4 °C) and high pH (pH 10). The AFM results show that peptoid nanosheets prepared with **7** template the growth of gold films and nanocrystals from aqueous gold atoms (Figure 8). The morphology of the gold nanostructures exhibits a strong dependence on the surface density, or interdomain spacing, of the surface-displayed peptide loops. Nanosheets displaying the maximum surface density of peptide loops trigger growth of a continuous metal film (on both sides of the nanosheet), with the thickness of the metal layer estimated to be 3 nm (per side) by AFM (Figure 8A). Considering that the peptoid nanosheet is only two molecules thick and electrically insulating, these trilayer composite materials hold promise as miniaturized supercapacitors for energy storage.[39] As the interdomain spacing between loops is increased, the gold deposited on the surface of the peptoid nanosheet becomes increasingly discontinuous, with a variety of morphologies, including agglomerated clusters (Figure 8B), a porous, mesh-like nanostructure (Figure 8C), and a distributed array of discrete gold "dots" (Figure 8D), accessible across the 1, 0.1, and 0.01% surface densities, respectively. Motivated by the recent interest in bottom-up assembly of ordered, 2D arrays of metal nanocrystals for surface-enhanced Raman sensors and plasmonic devices,[40] the optoelectronic properties of these metal–organic hybrid materials are currently under investigation.

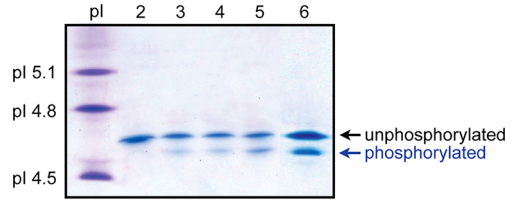

Figure 7. Isoelectric focusing (IEF) gel electrophoresis used to quantify the degree of phosphorylation of peptide-loop nanosheets by CK2α. Within an IEF gel, peptoid strands are separated based on isolectric point (p*I*), such that the phosphorylated polymer migrates farther (lower band, more acidic p*I*) than unphosphorylated starting material (upper band). Lane 1 contains IEF protein standard. Lanes 2–5 correspond to 15 μg of unstructured peptoid 5 reacted with varying concentration of CK2α. Lane 6 corresponds to peptoid 5 nanosheets (shown in Figure 6A) reacted with CK2α under identical conditions as lane 5. The amount of CK2α used in lanes 2–6 (with % conversion to phosphorylated product, listed in parentheses) was: 0 μg CK2α (0% phosphorylation), 1.0 μg (21%), 1.5 μg (24%), 2.0 μg (31%), and 2.0 μg (19%), respectively.

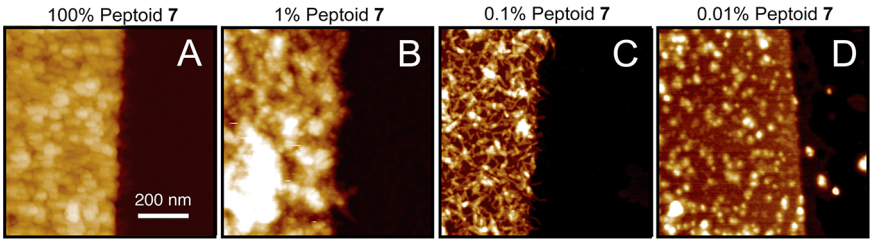

Figure 8. AFM images of gold-decorated peptoid nanosheets. The concentration of peptide loops displayed on the surface of the nanosheet was systematically varied, by preparing nanosheets from different mixing ratios of the gold-binding loop peptoid 7 and peptoid 8 as follows: (A) 100, (B) 1, (C) 0.1, and (D) 0.01% peptoid 7. Scale bar in (A) is same for all images.

CONCLUSION

Inspired by the way a linear sequence of amino acids encodes folded antibody domains, a linear polypeptoid sequence was designed to self-assemble into a peptoid nanosheet with a high density of molecular recognition loops displayed on the surface. Taking advantage of the peptoid's affinity for the air−water interface during peptoid nanosheet formation, loop-forming sequences were designed to preferentially display on the aqueous side of the interface, ultimately becoming the exterior surface of the nanosheet. The existence of loop domains on the surface of peptoid nanosheets was verified with AFM and powder XRD. Compression-induced peptoid loop formation at the air−water interface was confirmed by *in situ* monitoring of the air−water interface with surface pressure and XR measurements. The interior scaffolding of loop-displaying nanosheets was found to consist of an ordered, 2.8 nm thick peptoid bilayer, structurally identical to the bilayer of nonloop-displaying peptoid nanosheets. Peptide loop-displaying nanosheets were proven capable of molecular recognition by enzymes (proteases and CK2α), as well as of templating the growth of inorganic materials (gold metal) on the nanosheet surface.

Formation of a three-dimensional, antibody-like architecture from an information-rich, linear peptoid chain positions us one step closer toward extending the rules of protein folding to the world of synthetic materials. Moreover, the sequence design and protocol for nanosheet formation described in this work follows a simple mechanism (adsorption and compression of a peptoid monolayer at the air water interface), which is both amenable to exploring a combinatorial library of functional, hydrophilic peptide (or peptoid) inserts as well as readily scalable for automated, efficient production of functionalized peptoid nanosheets. Ongoing research is aimed at templating the assembly of other inorganic materials and exploiting the multivalency of these high surface area display materials. The ability to easily incorporate multifunctionality on the surface of a single peptoid nanosheet, through the display of both inorganic (gold) and organic (protein) recognition sites, combined with the exceptional stability of peptoids, makes loop-displaying peptoid nanosheets an especially promising platform for sensing and catalysis.

MATERIALS AND METHODS

Materials. Peptoid and peptoid−peptide hybrid oligomers were synthesized on an automated robotic synthesizer using the solid-phase submonomer method and purified by reverse-phase HPLC, as previously described.[14] Pronase Protease (Calbiochem) and recombinant, human CK2α (0.5 mg/mL, Calbiochem) were purchased from EMD Millipore. Novex pH 3−10 isoelectric focusing (IEF) gels (1.0 mm, 12 well), sample buffer, anode and cathode buffers were purchased from Invitrogen. The IEF gel protein standard (p*I* range: 4.45−9.6) was purchased from Bio-Rad. Adenosine 5-triphosphate disodium salt hydrate (ATP, ≥99%), monoclonal anti-phosphoserine−FITC antibody (2 mg/mL in 0.01 M PBS, pH 7.4 containing 1% BSA and 0.01% thimerosal), gold(III) chloride trihydrate (≥49.0% Au basis), and all other reagents were purchased from Sigma Aldrich.

Peptoid Nanosheet Preparation. Pure, lyophilized peptoid was dissolved in a 2:1 (v/v) mixture of DMSO/water to obtain a 2 mM peptoid stock solution stored at room temperature. In a clean, cylindrical 4 mL glass vial, 500 μL of nanosheet-forming solution (20 μM peptoid, 10 mM buffer) in Milli-Q water was prepared from the 2 mM peptoid stock solution. Nanosheets containing peptoid **5** (Table 1) were prepared using 2-amino-2-methyl-1,3-propandiol (AMPD), pH 9.0 buffer; all other nanosheets were prepared using Tris, pH 8.0 buffer. The density of peptide loops, displayed on the surface of the nanosheet, was systematically varied by preparing nanosheets from different mixing ratios of two peptoids (for example, from a solution containing a binary mixture of peptoid **1**/peptoid **5** in a 90%:10% molar ratio). To prepare the mixed nanosheet solution, appropriate aliquots of 2 mM peptoid stock solution of each peptoid sequence were added to the nanosheet-forming solution to achieve a total peptoid concentration of 20 μM (500 μL total volume). All vials were capped and then rotated from vertical to horizontal at room temperature, using a previously described[17] custom-built device that allows the wait time between vial rotation cycles to be set at 900 s.

Peptoid Nanosheet Characterization. Individual peptoid nanosheets were analyzed with atomic force microscopy (AFM) using an Asylum MFP-3D AFM. Prior to AFM analysis, the nanosheet solutions were dialyzed, using a 1 mL Spectra-Por Float-A-Lyzer device with 100 kD molecular weight cutoff (MWCO), overnight against pure Milli-Q water, to remove free peptoid strands and buffer salt. A 2 μL droplet of dialyzed nanosheet solution was transferred onto freshly cleaved mica and imaged with tapping mode AFM in ambient air. Powder X-ray diffraction data (Figure S1, Supporting Information) were collected at a multiple-wavelength anomalous diffraction and monochromatic macromolecular crystallography beamline, 8.3.1, at the Advanced Light Source located at Lawrence Berkeley National Laboratory. Beamline 8.3.1 has a 5 T single pole superbend source with an energy range of 5−17 keV. Data were collected with a 3 × 3 CCD array (ADSC Q315r) detector at a wavelength of 1.1159 Å. Data sets were collected with the detector 200 mm from the sample. Peptoid nanosheet solutions were concentrated 100-fold in an Amicon Ultra centrifugal filter (100 kD MWCO, Millipore) and then centrifuged at 13 200 rpm for 20 min. After removing the supernatant, the resulting peptoid nanosheet pellet was pipetted onto a Kapton mesh (MiTeGen). Data was processed with custom Python scripts. Optical imaging of nanosheets was performed under epifluorescence illumination with an Olympus IX81 inverted microscope, fitted with a Hamamatsu Orca CCD camera. Nile red, an environmentally sensitive dye whose fluorescence intensity increases substantially when it is localized in hydrophobic environments, was added to the nanosheet-containing solution at a final concentration of 0.5 μM, to stain nanosheets for imaging. Images were obtained by transferring a 2 μL aliquot of nanosheet solution onto porous 1% agarose gel, as previously described.[17]

Peptoid Monolayer Characterization. X-ray reflectivity measurements were conducted at the air−water interface using the liquid surface spectrometer at beamline 9-ID C of the Advanced Photon Source (Argonne National Laboratory, Chicago, IL). Using an incident X-ray wavelength of 0.920172 Å, data was collected over a range of photon momentum transfer $0.01 < q_z < 0.62$ Å^{-1}. The peptoid monolayer was adsorbed from a Langmuir trough containing either 20 μM peptoid **1** or 20 μM peptoid **3**, in 10 mM Tris, pH 8.0 buffer. The trough was enclosed inside a gastight chamber, with the incident and scattered X-ray beams passing through a kapton window. A system of Teflon tubing and valves

permitted the air in the canister to be purged with moist helium, as monitored by an oxygen sensor in the chamber. The trough was translated transverse to the beam by 1 mm, *i.e.*, the width of the incident X-ray beam, to expose a fresh portion of the sample to the beam after each reflectivity scan and so avoid any potential radiation damage to the peptoid monolayer. The raw X-ray reflectivity data files were reduced using C-Plot (Certified Scientific Software, Cambridge, MA), including normalization of the reflectivity data by the Fresnel function to eliminate the effects due to dynamical scattering from the water–air interface, leaving the kinematical scattering due to the presence of the peptoid monolayer at the interface. Subsequent processing was done with StochFit,[41] which uses the so-called box-refinement algorithm, a model-independent means for obtaining the electron-density profile of the monolayer that accounts for the observed reflectivity data.

Protein Binding Assays. For peptide loop recognition with protease, peptoid nanosheets displaying gold-binding peptide loops were prepared from a binary peptoid solution comprised of 50% peptoid **7** and 50% peptoid **8**. The nanosheets were spin-concentrated into 10 mM Tris, pH 7.5 buffer using a 0.5 mL Amicon Ultra centrifugal filter (100 kD MWCO, Millipore), such that the final volume of nanosheet concentrate was 100 μL and free peptoid strands were removed. A stock solution of 20 mg/mL Pronase, 4 mM $CaCl_2$ was prepared in Milli-Q water just prior to use. The 100 μL nanosheet concentrate was incubated with Pronase on an Thermomixer R (Eppendorf) set at 40 °C, 300 rpm for 20 h, in a total assay volume of 200 μL containing 0.25 mg/mL of Pronase, 4 mM $CaCl_2$, and 50 mM Tris pH 7.5 buffer. The same protocol was applied to control nanosheets without loops, made from 100% peptoid **8**. After incubation with Pronase, nanosheets were either dialyzed overnight, using a 1 mL Spectra-Por Float-A-Lyzer device with 100 kD MWCO, against 1 L of pH 7, phosphate buffered saline (to remove Pronase protein and cleaved peptide), in preparation for AFM analysis; or denatured into free peptoid strands (by pipetting 1 mL of acetonitrile into the 200 μL assay tubes and equilibrating at room temperature overnight), in preparation for matrix-assisted laser desorption/ionization mass spectrometry (Applied Biosystem/MDS SCIEX 4800 MALDI TOF/TOF Analyzer). For peptide loop recognition with CK2a, eight glass vials (500 μL per vial) of peptoid nanosheets displaying kinase-binding peptide loops were prepared from a binary peptoid solution comprised of 50% peptoid **5** and 50% peptoid **1**. The nanosheets were spin-concentrated into 10 mM Tris, pH 7.5 buffer using a 4 mL Amicon Ultra centrifugal filter (100 kD MWCO, Millipore), such that the final volume of nanosheet concentrate was 100 μL and free peptoid strands were removed. A 1.5× stock solution of kinase assay buffer (225 mM NaCl, 15 mM $MgCl_2$, 30 mM Tris pH 7.5, 3 mM DTT, 1.5 mM EGTA, 0.75 mM Na_3VO_4, 7.5 mM β-glycerophosphate) was prepared in Milli-Q water and placed on ice, just prior to use. The 100 μL nanosheet concentrate (or 1.5 μL of 2 mM peptoid stock solution, in the case of the unstructured, free peptoid control experiments) was incubated with CK2a in a stationary heat block (to minimize any nanosheet-forming agitation at the air–water interface of the unstructured, free peptoid control samples) set at 40 °C for 3 h, in a total assay volume of 300 μL containing 2 μg of CK2a, 200 μM ATP, 150 mM NaCl, 10 mM $MgCl_2$, 20 mM Tris pH 7.5, 2 mM DTT, 1 mM EGTA, 0.5 mM Na_3VO_4, and 5 mM β-glycerophosphate. After incubation with CK2a, nanosheets were either spin-concentrated to 50 μL, using a 0.5 mL Amicon Ultra centrifugal filter (100 kD MWCO, Millipore), and incubated on ice for 4 h with 1 μL of FITC-labeled anti-phosphoserine antibody, 15 μL of the nanosheet concentrate, 2 μL of 50 uM nile red, and 2 μL of 10× antibody buffer (500 mM HEPES pH 7.0, 1 M NaCl, 50 mg/mL bovine serum albumin), in preparation for immunofluorescence imaging; or denatured into free peptoid strands (by pipetting 15 μL of a 4% sodium dodecyl sulfate (SDS) stock solution into the 300 μL assay tubes and equilibrating at room temperature overnight), in preparation for isoelectric focusing (IEF) gel electrophoresis. Prior to IEF analysis, SDS was removed from all samples by spin-filtering each sample through a 0.5 mL Amicon Ultra centrifugal filter (Millipore, 3 kD MWCO, 10000*g* for 12 min), reconstituting the 50 μL filter concentrate in 450 μL of Milli-Q water, and repeating this spin-filtering procedure two more times.

Gold Nucleation Experiments. For peptide loop recognition with gold ions, peptoid nanosheets displaying gold-binding peptide loops were prepared from a binary peptoid solution comprised of X% peptoid **7** and (100 − X)% peptoid **8**, where X = 100, 1, 0.1, or 0.01%. The nanosheets were spin-concentrated into 10 mM potassium carbonate pH 10.0 buffer using a 0.5 mL Amicon Ultra centrifugal filter (100 kD MWCO, Millipore), such that the final volume of nanosheet concentrate was 100 μL and free peptoid strands were removed. A stock solution of the gold salt (0.1 μM $HAuCl_4$) was prepared in Milli-Q water and stored at room temperature. The 100 μL nanosheet concentrate, as well as a clean 4 mL glass vial containing 5 μL of gold stock solution in 395 μL of Milli-Q water, were equilibrated in a 4 °C cold room for 15 min. The 100 μL of nanosheet concentrate was injected into the vial of 400 μL of aqueous gold solution, and the vial was immediately capped and placed on a rotating platform for 60 min (to facilitate gentle mixing) inside the 4 °C cold room. The solution was then immediately transferred to a 1 mL Spectra-Por Float-A-Lyzer cartridge (100 kD MWCO) and dialyzed overnight against pure Milli-Q water, to remove gold and buffer salts prior to AFM analysis.

Conflict of Interest: The authors declare no competing financial interest.

Acknowledgment. The authors thank I. Kuzmenko, J. Holton, C. Proulx, T. Haxton, and R. Mannige for useful discussions and technical assistance. This project was funded by the Defense Threat Reduction Agency under Contract No. IACRO-B1144571. The work was conducted at the Molecular Foundry with support from the Advanced Light Source, at Lawrence Berkeley National Laboratory, both of which are supported by the Office of Science, Office of Basic Energy Sciences, U.S. Department of Energy, under Contract No. DE-AC02-05CH11231. Monolayer scattering experiments performed at the Advanced Photon Source at Argonne National Laboratory were supported by the U.S. Department of Energy, Office of Science, Office of Basic Energy Sciences, under Contract No. DE-AC02-06CH11357.

Supporting Information Available: Powder XRD and GIXD spectra, XR data, DKP crystal structure file for compound **9**, and isoelectric focusing gel results. This material is available free of charge *via* the Internet at http://pubs.acs.org

REFERENCES AND NOTES

1. Alberts, B.; Bray, D.; Lewis, J.; Raff, M.; Roberts, K.; Watson, J. D. The Functional Properties of Antibodies. In *Molecular Biology of the Cell*; Garland Science: New York, 1994.
2. Zheng, G.; Patolsky, F.; Cui, Y.; Wang, W. U.; Lieber, C. M. Multiplexed Electrical Detection of Cancer Markers with Nanowire Sensor Arrays. *Nat. Biotechnol.* **2005**, *23*, 1294–1301.
3. Kim, A.; Ah, C. S.; Park, C. W.; Yang, J.-H.; Kim, T.; Ahn, C.-G.; Park, S. H.; Sung, G. Y. Direct Label-Free Electrical Immunodetection in Human Serum Using a Flow-Through-Apparatus Approach with Integrated Field-Effect Transistors. *Biosens. Bioelectron.* **2010**, *25*, 1767–1773.
4. Binz, H. K.; Amstutz, P.; Pluckthun, A. Engineering Novel Binding Proteins From Nonimmunoglobulin Domains. *Nat. Biotechnol.* **2005**, *23*, 1257–1268.
5. Ruigrok, V. J. B.; Levisson, M.; Eppink, M. H. M.; Smidt, H.; van der Oost, J. Alternative Affinity Tools: More Attractive Than Antibodies? *Biochem. J.* **2011**, *436*, 1–13.
6. Gebauer, M.; Skerra, A. Engineered Protein Scaffolds as Next-Generation Antibody Therapeutics. *Curr. Opin. Chem. Biol.* **2009**, *13*, 245–255.
7. Bradbury, A. R. M.; Sidhu, S.; Dübel, S.; McCafferty, J. Beyond Natural Antibodies: the Power of *in Vitro* Display Technologies. *Nat. Biotechnol.* **2011**, *29*, 245–254.
8. Holliger, P.; Hudson, P. J. Engineered Antibody Fragments and the Rise of Single Domains. *Nat. Biotechnol.* **2005**, *23*, 1126–1136.

9. Nicaise, M.; Valerio-Lepiniec, M.; Minard, P.; Desmadril, M. Affinity Transfer by CDR Grafting on a Nonimmunoglobulin Scaffold. *Protein Sci.* **2004**, *13*, 1882–1891.
10. Koide, A.; Gilbreth, R. N.; Esaki, K.; Tereshko, V.; Koide, S. High-Affinity Single-Domain Binding Proteins with a Binary-Code Interface. *Proc. Natl. Acad. Sci. U. S. A.* **2007**, *104*, 6632–6637.
11. Luxenhofer, R.; Fetsch, C.; Grossmann, A. Polypeptoids: a Perfect Match for Molecular Definition and Macromolecular Engineering? *J. Polym. Sci., Part A: Polym. Chem.* **2013**, *51*, 2731–2752.
12. Lee, B.-C.; Chu, T. K.; Dill, K. A.; Zuckermann, R. N. Biomimetic Nanostructures: Creating a High-Affinity Zinc-Binding Site in a Folded Nonbiological Polymer. *J. Am. Chem. Soc.* **2008**, *130*, 8847–8855.
13. Chongsiriwatana, N. P.; Patch, J. A.; Czyzewski, A. M.; Dohm, M. T.; Ivankin, A.; Gidalevitz, D.; Zuckermann, R. N.; Barron, A. E. Peptoids That Mimic the Structure, Function, and Mechanism of Helical Antimicrobial Peptides. *Proc. Natl. Acad. Sci. U. S. A.* **2008**, *105*, 2794–2799.
14. Kudirka, R.; Tran, H.; Sanii, B.; Ki Tae, N.; Choi, P. H.; Venkateswaran, N.; Chen, R.; Whitelam, S.; Zuckermann, R. N. Folding of a Single-Chain, Information-Rich Polypeptoid Sequence Into a Highly Ordered Nanosheet. *Biopolymers* **2011**, *96*, 586–595.
15. Sun, J.; Zuckermann, R. N. Peptoid Polymers: a Highly Designable Bioinspired Material. *ACS Nano* **2013**, *7*, 4715–4732.
16. Nam, K. T.; Shelby, S. A.; Choi, P. H.; Marciel, A. B.; Chen, R.; Tan, L.; Chu, T. K.; Mesch, R. A.; Lee, B. C.; Connolly, M. D.; *et al.* Free-Floating Ultrathin Two-Dimensional Crystals From Sequence-Specific Peptoid Polymers. *Nat. Mater.* **2010**, *9*, 454–460.
17. Sanii, B.; Kudirka, R.; Cho, A.; Venkateswaran, N.; Olivier, G. K.; Olson, A. M.; Tran, H.; Harada, R. M.; Tan, L.; Zuckermann, R. N. Shaken, Not Stirred: Collapsing a Peptoid Monolayer to Produce Free-Floating, Stable Nanosheets. *J. Am. Chem. Soc.* **2011**, *133*, 20808–20815.
18. Butler, S. Z.; Hollen, S. M.; Cao, L.; Cui, Y.; Gupta, J. A.; Gutiérrez, H. R.; Heinz, T. F.; Hong, S. S.; Huang, J.; Ismach, A. F.; *et al.* Progress, Challenges, and Opportunities in Two-Dimensional Materials Beyond Graphene. *ACS Nano* **2013**, *7*, 2898–2926.
19. Govindaraju, T.; Avinash, M. B. Two-Dimensional Nanoarchitectonics: Organic and Hybrid Materials. *Nanoscale* **2012**, *4*, 6102–6117.
20. Chen, S.; Cao, Z.; Jiang, S. Ultra-Low Fouling Peptide Surfaces Derived From Natural Amino Acids. *Biomaterials* **2009**, *30*, 5892–5896.
21. Brault, N. D.; Gao, C.; Xue, H.; Piliarik, M.; Homola, J.; Jiang, S.; Yu, Q. Ultra-Low Fouling and Functionalizable Zwitterionic Coatings Grafted Onto SiO2 *via* a Biomimetic Adhesive Group for Sensing and Detection in Complex Media. *Biosens. Bioelectron.* **2010**, *25*, 2276–2282.
22. Vallee, A.; Humblot, V.; Pradier, C.-M. Peptide Interactions with Metal and Oxide Surfaces. *Acc. Chem. Res.* **2010**, *43*, 1297–1306.
23. Dickerson, M. B.; Sandhage, K. H.; Naik, R. R. Protein- and Peptide-Directed Syntheses of Inorganic Materials. *Chem. Rev.* **2008**, *108*, 4935–4978.
24. Sarikaya, M.; Tamerler, C.; Jen, A. K.; Schulten, K.; Baneyx, F. Molecular Biomimetics: Nanotechnologythrough Biology. *Nat. Mater.* **2003**, *2*, 577–585.
25. Houseman, B. T.; Huh, J. H.; Kron, S. J.; Mrksich, M. Peptide Chips for the Quantitative Evaluation of Protein Kinase Activity. *Nat. Biotechnol.* **2002**, *20*, 270–274.
26. Robinson, W. H.; DiGennaro, C.; Hueber, W.; Haab, B. B.; Kamachi, M.; Dean, E. J.; Fournel, S.; Fong, D.; Genovese, M. C.; Vegvar, H. E. N. de V.; *et al.* Autoantigen Microarrays for Multiplex Characterization of Autoantibody Responses. *Nat. Med.* **2002**, *8*, 295–301.
27. Kuenzel, E. A.; Mulligan, J. A.; Sommercorn, J.; Krebs, E. G. Substrate Specificity Determinants for Casein Kinase II as Deduced From Studies with Synthetic Peptides. *J. Biol. Chem.* **1987**, *262*, 9136–9140.
28. Kulp, J. L., III; Sarikaya, M.; Spencer Evans, J. Characterization of the Integral Sequence Repeat From the *E. coli* Gold Binding Protein, GBP-1. *J. Mater. Chem.* **2004**, *14*, 2325–2332.
29. Miller, S. M.; Simon, R. J.; Ng, S.; Zuckermann, R. N.; Kerr, J. M.; Moos, W. H. Proteolytic Studies of Homologous Peptide and N-Substituted Glycine Peptoid Oligomers. *Bioorg. Med. Chem. Lett.* **1994**, *4*, 2657–2662.
30. Miller, S. M.; Simon, R. J.; Ng, S.; Zuckermann, R. N.; Kerr, J. M.; Moos, W. H. Comparison of the Proteolytic Susceptibilities of Homologous L-Amino-Acid, D-Amino-Acid, and N-Substituted Glycine Peptide and Peptoid Oligomers. *Drug Dev. Res.* **1995**, *35*, 20–32.
31. Oestreicher, A. B.; DeGraan, P. N. E.; Schrama, L. H.; Lamme, V. A. F.; Bloemen, R. J.; Schotman, P.; Gispen, W. H. The Protein Kinase C Phosphosite(S) in B-50 (GAP-43) Are Confined to 15K Phosphofragemnets Produced by *Staphylococcus aureus* V8 Protease. *Neurochem. Int.* **1988**, *14*, 361–372.
32. Zwiers, H.; Verhaagen, J.; van Dongen, C. J.; de Graan, P. N. E.; Gispen, W. H. Resolution of Rat Brain Synaptic Phosphoprotein B-50 Into Multiple Forms by Two-Dimensional Electrophoresis: Evidence for Multisite Phosphorylation. *J. Neurochem.* **1985**, *44*, 1083–1090.
33. Abu-lawi, K. I.; Sultzer, B. M. Induction of Serine and Threonine Protein Phosphorylation by Endotoxin-Associated Protein in Murine Resident Peritoneal Macrophages. *Infect. Immun.* **1995**, *63*, 498–502.
34. Colfen, H.; Yu, S.-H. Biomimetic Mineralization/ Synthesis of Mesoscale Order in Hybrid Inorganic– Organic Materials *via* Nanoparticle Self-Assembly. *MRS Bull.* **2005**, *30*, 727–735.
35. Whittell, G. R.; Hager, M. D.; Schubert, U. S.; Manners, I. Functional Soft Materials From Metallopolymers and Metallosupramolecular Polymers. *Nat. Mater.* **2011**, *10*, 176–188.
36. Dong, Z.; Luo, Q.; Liu, J. Artificial Enzymes Based on Supramolecular Scaffolds. *Chem. Soc. Rev.* **2012**, *41*, 7890.
37. Matmor, M.; Ashkenasy, N. Peptide Directed Growth of Gold Films. *J. Mater. Chem.* **2011**, *21*, 968–974.
38. Wang, Z.; Chen, J.; Yang, P.; Yang, W. Biomimetic Synthesis of Gold Nanoparticles and Their Aggregates Using a Polypeptide Sequence. *Appl. Organomet. Chem.* **2007**, *21*, 645–651.
39. El-Kady, M. F.; Kaner, R. B. Scalable Fabrication of High-Power Graphene Micro-Supercapacitors for Flexible and on-Chip Energy Storage. *Nat. Commun.* **2013**, *4*, 1475.
40. Jones, M. R.; Osberg, K. D.; Macfarlane, R. J.; Langille, M. R.; Mirkin, C. A. Templated Techniques for the Synthesis and Assembly of Plasmonic Nanostructures. *Chem. Rev.* **2011**, *111*, 3736–3827.
41. Danauskas, S. M.; Li, D.; Meron, M.; Lin, B.; Lee, K. Y. C. Stochastic Fitting of Specular X-Ray Reflectivity Data Using StochFit. *J. Appl. Crystallogr.* **2008**, *41*, 1187–1193.